

**Multicomponent mutual diffusion in the warm, dense matter regime**A. J. White, C. Ticknor, E. R. Meyer, J. D. Kress, and L. A. Collins *Theoretical Division, Los Alamos National Laboratory, Los Alamos, New Mexico 87545, USA*

(Received 10 July 2019; published 30 September 2019)

We present the formulation, simulations, and results for multicomponent mutual diffusion coefficients in the warm, dense matter regime. While binary mixtures have received considerable attention for mass transport, far fewer studies have addressed ternary and more complex systems. We therefore explicitly examine ternary systems utilizing the Maxwell-Stefan formulation that relates diffusion to gradients in the chemical potential. Onsager coefficients then connect the macroscopic diffusion to microscopic particle motions, evinced in trajectories characterized by positions and velocities, through various autocorrelation functions (ACFs). These trajectories are generated by molecular dynamics (MD) simulations either through the Born-Oppenheimer approximation, which treats the ions classically and the electrons quantum-mechanically by an orbital-free density-functional theory, or through a classical MD approach with Yukawa pair-potentials, whose effective ionizations and electron screening length derive from quantal considerations. We employ the reference-mean form of the ACFs and determine the center-of-mass coefficients through a simple reference-frame-dependent similarity transformation. The Onsager terms in turn determine the mutual diffusion coefficients. We examine a representative sample of ternary mixtures as a function of density and temperature from those with only light elements (D-Li-C, D-Li-Al) to those with highly asymmetric mass components (D-Li-Cu, D-Li-Ag, H-C-Ag). We also follow trends in the diffusion as a function of number concentration and evaluated the efficacy of various approximations such as the Darken approximation.

DOI: [10.1103/PhysRevE.100.033213](https://doi.org/10.1103/PhysRevE.100.033213)**I. INTRODUCTION**

Warm, dense matter (WDM) designates an expansive material condition in which most or all of the constituents reside in a fluid state of some degree of ionization. This designation encompasses a broad variety of systems and environments as exemplified by planetary and stellar interiors and atmospheres, inertial confinement fusion (ICF), and intense laser interactions with materials. In most of these cases, the environment consists of a farrago of various components, which can include molecules, atoms, and ions of various species as well as electrons and transient combinations. To accurately model these macroscopic systems requires an intricate knowledge of the microscopic properties of the constituent materials, which include the equation-of-state (EOS), mass transport (diffusion and viscosity), thermal and electrical conduction, opacities, and stopping powers for mixtures.

An interesting example derives from the physical mechanisms associated with the implosion dynamics of ICF capsules driven by ultraintense laser fields [1]. For example, the inclusion of small amounts of the ablator material can deleteriously affect the efficiency of the burning of the deuterium-tritium fuel. Therefore, finding the most appropriate materials [2] from plastics as polystyrene, metals as beryllium, and carbon compounds as diamond and boron carbide requires a detailed knowledge of the EOS, the thermal conductivity, and the opacity of both the shell and resulting plasma. In addition, the deposition of heat from the slowing of the fusion-produced  $\alpha$  particles, as accounted for by the stopping power, determines the efficacy of the deposition process [3,4]. Finally, electrical and mass transport properties play a critical role in model-

ing the generation of fast electron beams from intense laser interactions with solids that produce hot, dense plasmas [5]. In addition, the mutual diffusion coefficient  $D$  and shear viscosity  $\eta$  govern the mass transport within hydrodynamic simulations and together with the mass density  $\rho$  determine the Schmidt number or matrix  $S_c = \frac{\eta}{\rho D}$  that characterizes mixing [6].

Another example encompasses the interiors of ice-giant planets such as Uranus and Neptune that may consist of a combination of methane (CH<sub>4</sub>), ammonia (NH<sub>3</sub>), and water (H<sub>2</sub>O) under high compression at temperatures of a few thousand Kelvin [7]. For these conditions, the constituents reside in a variety of complex states, especially since dissociation becomes possible. A particularly interesting state concerns superionic structures with one or more of the heavy species in a regular lattice while the lighter species (H) diffuses [8]. A knowledge of the EOS, thermal and electrical conduction, and mass transport become essential to understand such processes. Various studies of single [9–12], binary [13], and ternary [14] molecular species have provided insight into the structure and dynamics of planetary interiors not only in our solar system but also for the ever growing menagerie of exoplanets [15].

Most of these properties have undergone a thorough examination using a variety of models and *ab initio* methods. However, in the case of mutual diffusion, almost all studies in the WDM regime have focused on binary systems [16–25], which follow an exclusive formulation that does not encompass certain general features of ternary and higher-order systems. Thus, in this paper, we focus on ternary systems as better representative of the general behavior, mechanics,

and computational challenges of complex mixtures. The next section (Sec. II) develops the basic formalism for determining mutual diffusion coefficients from the products of molecular dynamics (MD) simulations, mainly the trajectories (time-dependent coordinates and velocities). We shall then discuss the basic formulations for these MD calculations in terms of two representations, both of which employ classical dynamics to advance the nuclei but utilize different treatments of the electrons. The first employs a classical Yukawa pair-potential with fixed parameters modified to approximate some of the quantum nature of the medium (Thomas-Fermi screening) while the second, an orbital-free density-functional theory (DFT), encompasses a full, self-consistent quantum mechanical treatment of the interacting electrons. The section concludes with a brief discussion of various analysis prescriptions. The third section (Sec. III) contains an analysis of the results from large-scale MD simulations for several representative ternary systems, consisting of low-mass components (D-Li-C) as well as highly asymmetric combinations (D-Li-Ag, H-C-Ag). This analysis focuses on the general trends in the behavior of the mutual diffusion coefficients for these ternary systems over a span of the WDM regime as well as technical issues. We make some concluding remarks in the final section, Sec. IV. Throughout the paper, we employ a mix of atomic and cgs units (1 au time:  $\tau_{\text{au}} = 2.42 \times 10^{-17}$  s, 1 au length: bohr  $\equiv a_B = 5.2917 \times 10^{-9}$  cm, and 1 au of energy: Hartree = 27.21 eV).

## II. MAXWELL-STEFAN AND FICKIAN DIFFUSION

We focus on two complementary approaches to multi-component diffusion [26–31], the Fickian and the Maxwell-Stefan, and present only a highly schematic description of the two formulations, mainly aiming at highlighting the most important aspects in relation to molecular dynamics simulations since the literature already abounds in detailed expositions [32–44]. We treat a multicomponent mixture of  $n_s$  species with a total number of atoms  $N = \sum_i N_i$ , a total mass  $M = \sum_i N_i m_i$ , a total number density  $n_a = N/V$ , and a mass density  $\rho = M/V$ , where  $V$  is the volume and the  $i$ th species has  $N_i$  atoms of mass  $m_i$ . The molar fraction is given by  $x_i = N_i/N$  such that  $\sum_i x_i = 1$  and the mass fraction  $\omega_i = N_i m_i / M$  with  $\sum_i \omega_i = 1$ .

The formulation due to Fick gives a more intuitive description closer to actual experimental arrangements of the diffusive process. The diffusion coefficient relates a change in a concentration to the resulting material flux as

$$J_i = -c_t \sum_j D_{ij}^f \nabla x_j \quad (1)$$

with  $J$  the molar flux,  $c_t$  the total molar concentration, and  $D_{ij}^f$  the Fickian diffusion coefficient.

On the other hand, the Maxwell-Stefan formulation [45,46] (MS) employs a driving force for diffusion given by the gradient of the chemical potential balanced by a friction force as

$$-\frac{1}{RT} \nabla \mu_i = \sum_{j \neq i} \frac{x_j (u_i - u_j)}{\mathcal{D}_{ij}}, \quad (2)$$

where  $R$  is the gas constant,  $T$  is the temperature, and  $\mu_i$  and  $u_i$  are the chemical potential and velocity of component  $i$  respectively. The MS diffusion coefficients, given by  $\mathcal{D}$ , represent an inverse friction coefficient. Recasting Eq. (2) in terms of a reference velocity  $u$  and a matrix  $\mathcal{B}$  leads to

$$-\frac{1}{RT} \nabla \mu_i = \sum_j x_j \mathcal{B}_{ij} (u_j - u), \quad (3)$$

where

$$(\mathcal{B})_{ii} = \frac{x_i}{\mathcal{D}_{i,n_s}} + \sum_{j \neq i} \frac{x_j}{\mathcal{D}_{ij}}, \quad (4)$$

$$(\mathcal{B})_{ij} = -x_i \left( \frac{1}{\mathcal{D}_{ij}} - \frac{1}{\mathcal{D}_{i,n_s}} \right). \quad (5)$$

Inverting Eqs. (5) then yields the MS diffusion coefficients [37].

Since the two approaches are complementary, the respective mutual diffusion coefficients are related by a simple matrix operation,

$$\mathbf{D}^f = \mathcal{B}^{-1} \mathbf{Q}, \quad (6)$$

where  $\mathbf{Q}$  is a matrix determined solely from thermodynamical considerations, such as by Kirkwood-Buff integrals [43,44] or binary-ion models [47]. The Fickian formulation gives  $(n_s - 1)(n_s - 1)$  independent diffusion coefficients while the Maxwell-Stefan produces only  $n_s(n_s - 1)/2$  given that  $\mathcal{D}_{ij} = \mathcal{D}_{ji}$ . We shall restrict this paper to the Maxwell-Stefan approach, given its sole reliance on the microscopic dynamical properties, for example the positions and velocities of the atoms extracted directly from an MD simulation. An exposition on the determination of the  $\mathbf{Q}$  quantity appears in the previously cited sources.

### A. Maxwell-Stefan diffusion and molecular dynamics

#### 1. General formulation

We return now to the MS formulation and relate its diffusion coefficients to the results of MD simulations. From these simulations, we produce a trajectory that contains the three-dimensional (3D) coordinates  $[\mathbf{r}_\alpha^i(t)]$  and velocities  $[\mathbf{v}_\alpha^i(t)]$  for each particle  $\alpha$  of species  $i$  at a given time  $t$ . The MD coordinates and velocities are advanced by a time step  $\delta_t$  for  $n_t$  steps for a total time of  $t_{\text{max}} = n_t \delta_t$ . A similar construction to Eq. (3) defines the phenomenological Onsager coefficients  $\Lambda_{ij}$  by

$$x_i u_i = -\frac{1}{RT} \sum_j \Lambda_{ij} \nabla \mu_j, \quad (7)$$

which in turn can be directly related in the linear-response limit to the MD trajectory through either a mean-squared displacement (MSD) or velocity autocorrelation function (VACF) as

$$\Lambda_{ij} = \frac{1}{6} \frac{1}{N \Delta t} \langle [\mathbf{R}_i(t + \Delta t) - \mathbf{R}_i(t)] \cdot [\mathbf{R}_j(t + \Delta t) - \mathbf{R}_j(t)] \rangle, \quad (8)$$

or

$$\Lambda_{ij}^R(t) = \frac{1}{3} \frac{1}{N} \int_0^t dt' \langle \mathbf{V}_i(0) \cdot \mathbf{V}_j(t') \rangle, \quad (9)$$

such that

$$\Lambda_{ij}^R(t) \xrightarrow{t \rightarrow \infty} \Lambda_{ij}^R, \quad (10)$$

where the superscript  $R$  designates a particular reference frame. Since the MSD form depends on the difference between the coordinates of the same particle at different times, this specific formulation is *independent* of the choice of reference frame; however, the VACF form is not. The angular brackets represent an ensemble average and

$$\begin{aligned} \mathbf{R}_i(t) &= \sum_{\alpha=1}^{N_i} \mathbf{r}_\alpha^i(t) \\ \mathbf{V}_i(t) &= \sum_{\alpha=1}^{N_i} \mathbf{v}_\alpha^i(t). \end{aligned} \quad (11)$$

The positions and velocities in Eq. (11) refer to a particular reference frame with molecular dynamics generally, as in this paper, favoring the center-of-mass (c.m.) such that  $\mathbf{V}_{\text{c.m.}}(t) = \sum_{i=1}^{n_s} \omega_i \mathbf{V}_i(t)$  with a similar expression for the positions. For comparison purposes, we shall sometimes employ the normalized VACF, given by dividing the integrand of Eq. (9) by  $N_{ij} = \langle \mathbf{V}_i(0) \cdot \mathbf{V}_j(0) \rangle$ .

A more compact approach utilizes the relative-mean velocity autocorrelation functions (RM-VACF), which are independent of the specific reference frame [48]:

$$\Lambda_{ij}^{\text{RM}}(t) = \frac{1}{3} \frac{1}{N} \int_0^t dt' \langle [\mathbf{V}_i(t') - \mathbf{V}_j(t')] \cdot [\mathbf{V}_i(0) - \mathbf{V}_j(0)] \rangle. \quad (12)$$

Any reference-frame specific Onsager coefficient derives then from a simple matrix transformation

$$\mathbf{\Lambda}^R = -\frac{1}{2} \mathbf{S}^R \mathbf{\Lambda}^{\text{RM}} \tilde{\mathbf{S}}^R, \quad (13)$$

where  $\mathbf{\Lambda}^R$  and  $\mathbf{\Lambda}^{\text{RM}}$  represent matrices composed of the elements of Eqs. (8) or (9) and Eq. (12), respectively; the tilde designates the transpose; the  $R$  indicates the reference frame dependence; and the  $S$ -matrix has the simple form

$$[\mathbf{S}^R]_{\alpha\beta} = \delta_{\alpha\beta} - g_\beta, \quad (14)$$

where  $g_\beta$  carries the RF dependency [49]. For the center-of-mass or barycentric frame, we have  $g_\beta = \omega_\beta$ , the mass fraction. The relative velocity form  $\mathbf{\Lambda}^{\text{RM}}$  is symmetric by construction with the diagonal containing zeros [ $\Lambda_{ii} = 0$ ] and is formally equivalent to Eq. (9).

Since the remaining formulation relating the ACFs to the diffusion coefficients applies for any reference frame, we drop the superscript  $R$  in the following analysis. The Onsager coefficients also obey certain symmetry rules

$$\begin{aligned} \Lambda_{ij} &= \Lambda_{ji} \\ \sum_i m_i \Lambda_{ij} &= 0. \end{aligned} \quad (15)$$

The second equation simply reflects that the center-of-mass velocity for the total system is zero and can be used to relate the off-diagonal Onsager coefficients to their diagonal counterparts:

$$\Lambda_{ij} = \frac{1}{2} [a_k \Lambda_{kk} - a_i \Lambda_{ii} - a_j \Lambda_{jj}] \quad (16)$$

such that  $k \neq i, j$  and  $a_k = [m_k^2 / (m_i m_j)]$ ;  $a_i = m_i / m_j$ ;  $a_j = m_j / m_i$ . A similar relation holds for the VACs.

We can then define, through some algebraic manipulations, a matrix  $\mathbf{\Delta}$  such that [36]

$$\mathbf{\Delta} = \mathbf{B}^{-1}, \quad (17)$$

$$(\mathbf{\Delta})_{ij} = (1 - x_i) \left[ \frac{\Lambda_{ij}}{x_j} - \frac{\Lambda_{in_s}}{x_{n_s}} \right] - x_i \sum_{k=1, k \neq i}^{n_s} \left[ \frac{\Lambda_{kj}}{x_j} - \frac{\Lambda_{kn_s}}{x_{n_s}} \right]. \quad (18)$$

From the  $\mathbf{B}$  matrix, we determine the MS diffusion coefficients. For example, for a binary system ( $n_s = 2$ ), we have

$$\mathcal{D}_{12} = \Delta_{11} = \frac{x_2}{x_1} \Lambda_{11} + \frac{x_1}{x_2} \Lambda_{22} - \Lambda_{12} - \Lambda_{21}, \quad (19)$$

and for a ternary system ( $n_s = 3$ ),

$$\begin{aligned} \mathcal{D}_{12} &= \frac{1}{B_{11} - \left(\frac{x_1 + x_3}{x_1}\right) B_{12}} \\ \mathcal{D}_{13} &= \frac{1}{B_{11} + \left(\frac{x_2}{x_1}\right) B_{12}} \\ \mathcal{D}_{23} &= \frac{1}{B_{22} + \left(\frac{x_1}{x_2}\right) B_{21}}. \end{aligned} \quad (20)$$

We observe that the  $\mathbf{B}$  matrix derives from the inverse of the  $\mathbf{\Delta}$  matrix, which in turn has a complicated dependence on many of the Onsager coefficients  $\Lambda_{ij}$ . Only the binary case though provides an exception; using the relationships in Eqs. (15), we can rewrite Eq. (19) as

$$\mathcal{D}_{12} = - \left[ \left(\frac{x_2}{x_1}\right)^2 + \left(\frac{x_1}{x_2}\right)^2 + 2 \right] \Lambda_{12}. \quad (21)$$

Before leaving this section, we present a brief summary of the prescription for determining the diffusion coefficients from the results of the MD simulations. First, we perform a series of MD simulations for a particular sample of species at set concentrations that produce trajectories consisting of a collection of the positions and velocities of particles [ $\mathbf{r}_\alpha^i(t)$ ;  $\mathbf{v}_\alpha^i(t)$ ,  $i = 1, n_s$ ,  $\alpha = 1, N_i$ ] at each time step over the span of the temporal propagation. Second, from the trajectories, we determine species-specific coordinations [ $\mathbf{R}_i(t)$ ;  $\mathbf{V}_i(t)$ ] by summing over the particles within a given component [Eq. (11)], which in turn determine the autocorrelation functions and the reference-frame-independent (relative mean) Onsager coefficients  $\Lambda_{ij}^{\text{RM}}$  through Eq. (8) and (12). Third, from the RM Onsager coefficients, we can then construct the appropriate Onsager coefficients for a particular reference frame (e.g., center-of-mass) through a simple similarity transformation [Eq. (13)]. Finally, a combination of these Onsager coefficients determines the  $\mathbf{\Delta}$  and  $\mathbf{B}$  matrices [Eq. (18)] from which the mutual diffusion coefficients  $\mathcal{D}_{ij}$  emerge [Eq. (5)].

## 2. Darken relations

Neglecting the cross-correlation terms in the Onsager coefficients generates the Darken relationships [32,37] for the

mutual diffusion coefficients in terms of the molar fractions and self-diffusion coefficients  $D_i$ :

$$D_i = \frac{1}{3} \frac{1}{N_i} \int dt \left\langle \sum_{\alpha=1}^{N_i} \mathbf{v}_\alpha^i(0) \cdot \mathbf{v}_\alpha^i(t) \right\rangle. \quad (22)$$

The self-diffusion only depends on contributions  $\mathbf{v}_j^i(0) \cdot \mathbf{v}_j^i(t)$  of the same particle of the same species. The full mutual diffusion coefficient additionally includes the cross-correlation terms between different particles of the same and of different species.

For the binary case, we have

$$\mathcal{D}_{12} = x_2 D_1 + x_1 D_2, \quad (23)$$

and for the ternary and higher systems,

$$\mathcal{D}_{ij} = \frac{D_i D_j}{D_{\text{mix}}}, \quad (24)$$

$$\frac{1}{D_{\text{mix}}} = \sum_i^{n_s} \frac{x_i}{D_i}. \quad (25)$$

We note though that the self-diffusion coefficients in the Darken formulas are those for the *fully mixed system*. Prescriptions exist to relate these to the self-diffusion coefficients for pure systems [36].

The ability to utilize the Darken approximations provides distinct computational advantages in determining mutual diffusion coefficients, which, like viscosity, are properties of the entire system while self-diffusion coefficients arise from single-atom correlation functions that can be averaged further to reduce the statistical error. In MD simulations, the statistical error or uncertainty [42]  $\epsilon$  for a system property that obeys Gaussian statistics goes as

$$\epsilon \approx \sqrt{\frac{2\tau}{T_{\text{traj}}}}, \quad (26)$$

where  $\tau$  represents a correlation time and  $T_{\text{traj}}$  the temporal length of the trajectory. The longest 1/e-folding time of the VACFs associated with the Onsager coefficients [Eq. (9)] gives a reasonable choice for  $\tau$ . The statistical error in the self-diffusion is reduced by an additional  $\frac{1}{\sqrt{N_i}}$ . Therefore, for 100 atoms, the self-diffusion will have an order of magnitude better statistical accuracy than the mutual diffusion for the same length of trajectory assuming that the correlation times are comparable. A few studies of ternary mixtures at ambient conditions for chemical systems have obtained good agreement ( $\sim 25\%$ ) between the Darken and full-simulation results [36,37].

## B. Molecular dynamics

We perform both classical and quantum molecular dynamics [50] simulations in the  $NVT$  ensemble for two conventions. In the first case, we fix the mass density and concentrations, which in turn sets the number density  $n_a$ . In the second convention, we fix the concentrations and the initial pressure, which determines the mass density. The MD simulation starts from this initial condition and evolves according to a  $NVT$  ensemble. The details of this prescription appear in references [22,23]. In both cases, a constant temperature is

maintained either by a simple velocity-scaling scheme [50] or by an isokinetic thermostat [51]. We have tested the efficacy of these ensembles by comparing to a collection of trajectories propagated according to a microcanonical ( $NVE$ ) ensemble and found only small differences in the properties.

The MD simulations produce a trajectory that contains the positions and velocities of all particles as a function of time step. For short trajectories, we can produce a single long file that is parsed to give uncorrelated segments for the determination of the VAC and MSD functions. However, for longer times, a more efficient approach dictates running simultaneously (in parallel) a number of uncorrelated short segments. Combining these then gives an average value to the AC functions and consequently the mutual diffusion coefficients. The computational benefit of such a scheme comes from the production of a long trajectory on the time scale of a shorter one.

### 1. Classical: Yukawa MD

We performed classical molecular dynamics simulations using a Yukawa pair-potential [52]:

$$V_{\alpha\beta}(r_{\alpha\beta}) = \frac{Z_\alpha Z_\beta e^2}{r_{\alpha\beta}} e^{-r_{\alpha\beta}/\lambda_e}, \quad (27)$$

where  $Z_\alpha e$  is the effective charge of atom  $\alpha$  of the species  $i$ ;  $\lambda_e$  and  $r_{\alpha\beta}$  are the electron screening length and the distance between atoms  $\alpha$  and  $\beta$ , respectively. The Yukawa parameters derive from an electron pressure matching scheme [16,53] for a fixed mass density, number concentration, and temperature. The mass density sets the total volume  $V$ , and the concentration determines the individual atom numbers ( $N_i = x_i N$ ). The atom volumes  $v_i$  are symmetrically varied until the electronic pressures match ( $P_i = P, \forall i$ ), subject to the constraint that  $V = \sum_i v_i$ . This condition in turn sets the partial atomic number density  $n_a^i = N_i/v_i$ . We employ a regularization prescription [53] to determine the pressures and the effective charge  $Z_i$  for each species. The scheme resembles average-atom models that treat a representative component in a plasma determined by a density and temperature. A linearized Thomas-Fermi theory [20,54] dictates the screening length  $\lambda_e$  based on the total electron density  $n_e = \sum_i Z_i n_a^i$ . Such pressure-matching schemes, also referred to as additive-volume and Amagat, have received some recent experimental support [55]. We solved the classical equation of motion by a velocity Verlet algorithm [50] and also employed the LAMMPS package [56] for the parallel implementation. Our Yukawa MD simulation results for diffusion and other properties agree well with several other studies: Ohta and Hamaguchi [52] for a single species and Stanton and Murillo [20] for binary systems.

### 2. Quantum: Orbital-free MD

For the quantal case, we invoke the Born-Oppenheimer approximation and separate the electronic and nuclear motions. The  $N$  nuclei move according to classical equations of motion (EOM) in response to a force on the ion from the interactions with other ions and a quantal contribution from the  $N_e$  electrons at a fixed ion configuration  $\{\mathbf{R}_i, i = 1, N\}$ . The force due to the electrons derives from the minimization of a free-energy functional in terms of the electron density  $n_e(\mathbf{r})$ ,

arising from finite-temperature orbital-free density functional theory (OF-DFT) [53] of the form:

$$F_e[n_e] = F_0[n_e] + U_{en}[n_e] + U_{ee}[n_e] + F_{xc}[n_e], \quad (28)$$

in which  $F_0$  is the Thomas-Fermi-Perrot finite-temperature noninteracting free energy [57],  $U_{en}$  is the electron-ion interaction from a regularization prescription [53],  $U_{ee}$  is the electron-electron Hartree contribution, and the exchange-correlation term  $F_{xc}$  comes from a local density Perdew-Zunger form [58]. The technique has proven highly effective in spanning the WDM regime, producing equilibrium mass transport quantities such as viscosity and diffusion as well as equations of state for both single and multicomponent dense plasmas [16,17,59–61] that agree well with the computationally more intense Kohn-Sham (KS) DFT at low temperatures [53,60–63] and with simpler models such as the one-component plasma at high temperatures [53]. Specifically, for LiH and LiD, the OF and KS MD results agree to within 10–15% over a range of densities from solid ( $0.79 \text{ g/cm}^3$ ) to 4 times compressed and temperature from 2 to 10 eV for mass transport coefficients [60] and equation of state [62].

### C. Analysis

Since unlike self-diffusion, the mutual diffusion coefficients represent bulk properties, they can exhibit considerable sensitivity to the prescriptions for evaluating the Onsager coefficients through the integral of the VACF in Eq. (9) or the derivative of the MSD in Eq. (8). We have found in previous studies [16,64] that fitting the functions or their integrals to simple analytical forms can reduce this sensitivity. As an example of the former, we consider for the Yukawa model a D-Li-C 1:1:1 by number mixture of 399 atoms at 100 eV and  $10 \text{ g/cm}^3$  and display in Fig. 1 the normalized VACFs associated with the RM Onsager coefficients as a function of time for a trajectory of  $6 \times 10^6$  time steps of length 0.5 au. The two Onsager coefficients that connect the light species to the heavy (DC and LiC) have almost exactly the same behavior while the light-light (DLi) coefficient exhibits a considerably different trend. By employing the combination of a gaussian for short times and an exponential  $[\exp(-t/\tau_o)]$  for the long decay, we can determine a fit to within better than 10% for all three VACFs. The largest decay or  $1/e$ -folding time  $\tau_o$  will, in turn reflect the statistical error  $\epsilon$ . In our example, the decay times are  $\approx 280$  au for DLi and  $\approx 420$  au for DC and LiC. Integrating the analytical form and multiplying by the norm  $N_{ij}$  produces the total Onsager coefficient  $\Lambda_{ij}^{\text{RM}}$ . Equation (13) then determines the specific reference-frame Onsager coefficients from which the final mutual diffusion coefficients arise. We could also calculate the diffusion coefficients directly from the RF VACFs. As an example, we display the unnormalized coefficients  $\Lambda_{ij}^{\text{R}}(t)$  also in Fig. 1. However, generally the RM coefficients provide a more flexible and stable ground for analysis.

Another strategy fits the time-dependent integral  $\Lambda_{ij}(t)$  to a basic form [16]

$$\Lambda_{ij}(t) = A_o[1 - \exp(-t/\tau_o)], \quad (29)$$

where  $t \rightarrow \infty$ ,  $\Lambda_{ij}(t) \rightarrow \Lambda_{ij} = A_o$ , from which we extract Onsager values. We display an example of this technique in

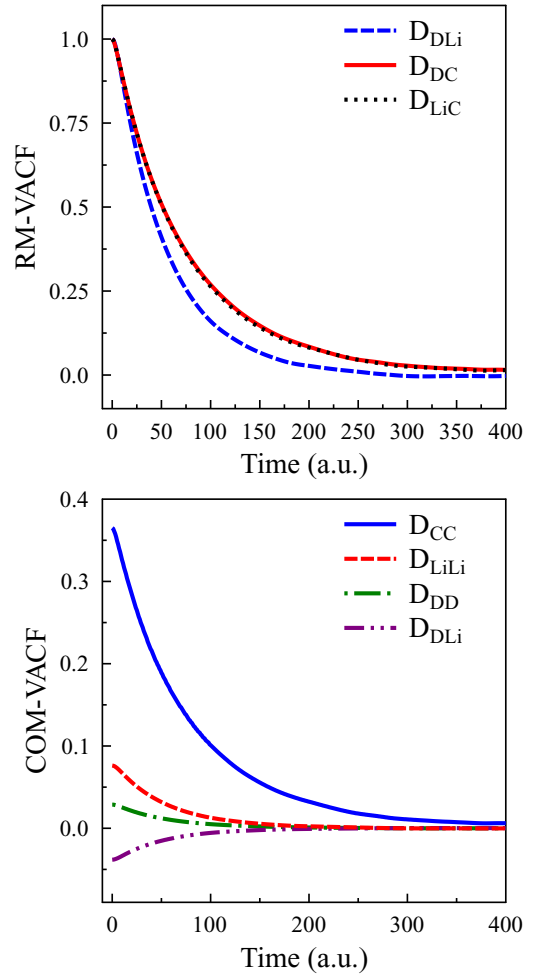


FIG. 1. Upper panel: Normalized velocity autocorrelation functions (VAC) as a function of time associated with the RM Onsager coefficients  $\Lambda_{ij}^{\text{RM}}$  for the Yukawa potential for a ternary 1:1:1 mixture of C, Li, and D at  $10 \text{ g/cm}^3$  and 100 eV. Curves: DLi (dashed blue line), DC (solid red line), and LiC (within the DC line width). Lower panel: Unnormalized center-of-mass velocity autocorrelation (c.m.-VAC) as a function of time for same case as in upper panel. Curves: CC (solid blue line), LiLi (red long-dashed line), DD (green dash-dotted line), DLi (purple dash-double-dot line), and DC and CLi within the DLi width.

Fig. 2 for the RM Onsager coefficients for DLi, DC, and LiC in a classical simulation with a Yukawa potential for the same D-Li-C mixture discussed in the previous paragraph. The fit gives a value for  $\Lambda_{\text{DLi}}^{\text{RM}}$  of  $4.24 \times 10^{-2}$  in line with the integrated value of  $4.21 \times 10^{-2}$ . The decay time is 270 au in excellent agreement with the VACF fits. We emphasize that these analysis prescriptions only apply once the system has reached a stable equilibrium. Also, in other temperature and density domains, more complex fitting prescriptions may apply [64].

### III. SIMULATIONS

In this section, we discuss the behavior of the mutual diffusion coefficients as a function of density and temperature for a selection of ternary systems using both the Yukawa and

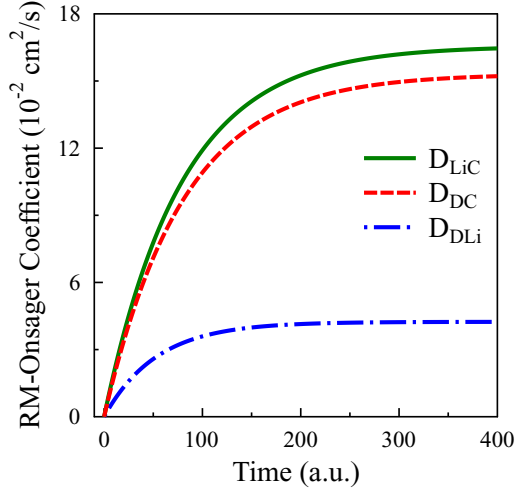


FIG. 2. Onsager coefficient  $\Lambda_{ij}(t)$  as a function of time for Yukawa potential for a ternary 1:1:1 mixture of C, Li, and D at  $10 \text{ g/cm}^3$  and  $10 \text{ eV}$ . Curves: LiC (green solid line); DC (red dashed line); DLi (blue dash-dotted line). The fits lie within the line widths.

OFMD formulations. We first focus on several representative cases of systems with three relatively light components (D-Li-C) and with two light and one very heavy member (D-Li-Ag). We then examine the behavior of the mutual diffusion coefficients for a composite sample of two light species (D, Li) as a function of the third heavier component (C, Al, Cu, and Ag). Finally, we shall examine a series of D-Li-C and H-C-Ag simulations as a function of concentration, temperature, and density.

## A. Representative ternary systems

### 1. D-Li-C

We perform Yukawa MD simulations on the representative system of D-Li-C (1:1:1) with 399 atoms at a density of  $10 \text{ g/cm}^3$  for temperatures from 10 to 300 eV. The effective charges and electron screening length all gradually rise with increasing temperature as indicated in Table I. Time steps varied between 0.25 au (300 eV) and 1 au (10 eV). Trajectories of length  $10^4$  time steps typically converged the self-diffusion coefficients to better than a few percent in agreement with the estimated statistical error  $\epsilon$ . However, the mutual diffusion

TABLE I. Effective charge ( $Z_\alpha$ ) and electron screening length ( $\lambda_e$ ) for the Yukawa potential as a function of temperature at  $10 \text{ g/cm}^3$  for representative cases for carbon (C), lithium (Li), deuterium (D), and silver (Ag); Li and D for equal concentrations by number.

| $T$ (eV) | $Z_C$    | $Z_{Li}$ | $Z_D$ | $\lambda_e$ |
|----------|----------|----------|-------|-------------|
| 10       | 3.0      | 1.9      | 0.80  | 0.7         |
| 100      | 4.0      | 2.4      | 0.90  | 0.92        |
| 300      | 5.1      | 2.7      | 0.96  | 1.7         |
| $T$ (eV) | $Z_{Ag}$ | $Z_{Li}$ | $Z_D$ | $\lambda_e$ |
| 100      | 11.7     | 2.4      | 0.91  | 1.22        |
| 400      | 22.7     | 2.8      | 0.97  | 1.75        |

coefficients require much longer temporal integrations and considerable care in managing the error. Typical correlation times taken from the VAC Onsager coefficients have values around 50–200 au, giving a statistical error of about 5% for a trajectory of  $10^5$  steps. We find, though, that this error can be misleading in determining the actual accuracy and convergence of the mutual coefficients. Therefore, to reduce the error to below a few percentages requires very long trajectories of  $10^6 - 10^7$  time steps. The origins of this behavioral difference between viscosity and mutual diffusion are not entirely clear since both represent bulk properties of the medium. Viscosity involves a sum over all the species and components of the stress ACF while mutual diffusion encompasses a more complicated scheme of manipulations. The Onsager coefficients incorporate sums over particles in pairs of species interacting within the whole system. These coefficients in turn determine the mutual diffusion through a set of operations that involve differences [Eqs. (18) and (20)], which may require a higher degree of accuracy to resolve. Some limited insight, as quantified later, emerges from the observation that the root-mean-square error for the Onsager coefficients is a factor of two or more smaller than those for the mutual diffusion coefficients themselves. We also note that the largest errors occur for the coefficient connecting the lightest two species. Interestingly, the need for such long trajectories also arises in determining mutual diffusion coefficients in chemical engineering applications [41] of multicomponent liquids at ambient conditions.

We have also performed a few tests for the 1:1:1 case with a total number of atoms of 900; the results indicate that calculations with 399 atoms appear reasonably well converged with a maximum difference of 10% in the mutual diffusion coefficients. Table II summarizes the results for the Yukawa MD simulations of the self-diffusion and mutual diffusion

TABLE II. Classical MD simulations for self- and mutual diffusion coefficients in a ternary system containing equal number concentrations of carbon (C), lithium (Li), and deuterium (D) interacting through Yukawa potentials. For each temperature, the top line gives the self-diffusion  $D_i$  and mutual diffusion  $D_{ij}$  coefficients in units of  $\text{cm}^2/\text{s}$  calculated from the MD trajectory with 399 atoms. The lower line gives the Darken values from Eq. (25). The Onsager coefficients were calculated from the VAC form. Power of 10 given in brackets.

| $T$ (eV) | $D_C$   | $D_{Li}$ | $D_D$   | $D_{CLi}$ | $D_{CD}$ | $D_{LiD}$ |
|----------|---------|----------|---------|-----------|----------|-----------|
| 10       | 6.6[−3] | 9.4[−3]  | 2.6[−2] | 6.3[−3]   | 1.8[−2]  | 2.5[−2]   |
|          | 6.1[−3] | 1.7[−2]  | 2.5[−2] |           |          |           |
| 20       | 1.4[−2] | 2.2[−2]  | 7.7[−2] | 1.4[−2]   | 4.9[−2]  | 7.7[−2]   |
|          | 1.4[−2] | 4.6[−2]  | 7.4[−2] |           |          |           |
| 40       | 2.6[−2] | 4.2[−2]  | 1.6[−1] | 2.6[−2]   | 9.8[−2]  | 1.6[−1]   |
|          | 2.5[−2] | 9.2[−2]  | 1.5[−1] |           |          |           |
| 60       | 3.5[−2] | 6.1[−2]  | 2.5[−1] | 3.4[−2]   | 1.3[−1]  | 2.6[−1]   |
|          | 3.5[−2] | 1.4[−1]  | 2.5[−1] |           |          |           |
| 80       | 4.2[−2] | 7.5[−2]  | 3.5[−1] | 4.4[−2]   | 2.0[−1]  | 3.6[−1]   |
|          | 4.2[−2] | 2.0[−1]  | 3.5[−1] |           |          |           |
| 100      | 5.1[−2] | 9.5[−2]  | 4.6[−1] | 4.9[−2]   | 2.7[−1]  | 4.7[−1]   |
|          | 5.2[−2] | 2.5[−1]  | 4.6[−1] |           |          |           |
| 300      | 1.2[−1] | 2.9[−1]  | 2.2[+0] | 1.3[−1]   | 1.1[+0]  | 2.4[+0]   |
|          | 1.4[−1] | 1.1[+0]  | 2.6[+0] |           |          |           |

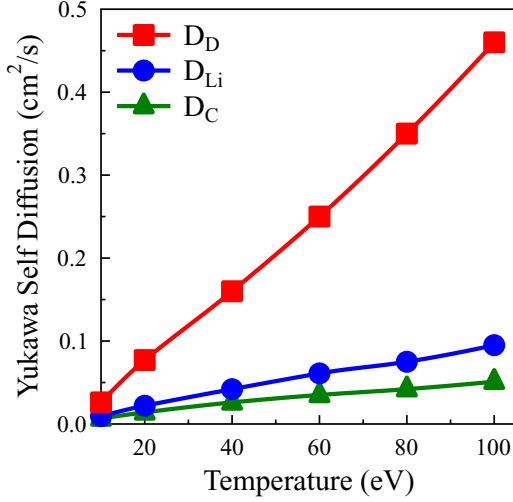


FIG. 3. Self-diffusion coefficients as a function of temperature for Yukawa model for a ternary 1:1:1 mixture DLiC mixture at  $10 \text{ g/cm}^3$  for 399 atoms with C (green triangle), Li (blue circle), and D (red square).

coefficients as well as the Darken approximation. These results are graphically displayed in Figs. 3 and 4. The Darken formula gives a reasonable approximation to the mutual diffusion coefficients with the largest error less than 10%. This finding agrees with other studies on binary systems of CH [65], LiH [18,60], and PuH [21] using the OFMD method.

In addition, we executed simulations with the OFMD prescription for the representative ternary mixture of equal numbers of C, Li, and D atoms at  $10 \text{ g/cm}^3$  for temperatures ranging from 10 to 100 eV for samples with 90 and 150 atoms, the results of which appear in Table III and evince excellent convergence in sample size. The time steps varied from 4 au (10 eV) to 1 au (100 eV) with trajectories of  $1 \times 10^5$

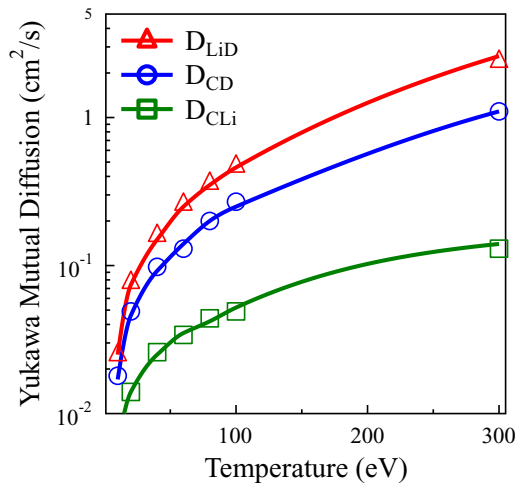


FIG. 4. Ternary mutual diffusion coefficients  $D_{ij}$  as a function of temperature for a Yukawa model at  $10 \text{ g/cm}^3$  for a 1:1:1 mixture with 399 atoms of C, Li, and D: Comparison of full Maxwell-Stefan (symbols) and Darken (lines) formulations.  $D_{\text{CLi}}$  (green),  $D_{\text{CD}}$  (blue),  $D_{\text{DLi}}$  (red).

TABLE III. OFMD simulations for self and mutual diffusion coefficients as function of temperature for a ternary system containing carbon (C), lithium (Li), and deuterium (D) in a 1:1:1 number ratio at  $10 \text{ g/cm}^3$  for 150 atoms. For each temperature, the first line gives the self-diffusion  $D_i$  and the mutual diffusion coefficients  $D_{ij}$  for the Darken approximation. The second line for 40 eV and 100 eV gives the self- and mutual diffusion coefficients for the *full ternary* MD simulations with 90 atoms. Power of 10 given in brackets.

| $T$ (eV) | $D_C$   | $D_{\text{Li}}$ | $D_D$   | $D_{\text{CLi}}$ | $D_{\text{CD}}$ | $D_{\text{DLi}}$ |
|----------|---------|-----------------|---------|------------------|-----------------|------------------|
| 10       | 4.1[−3] | 6.2[−3]         | 1.7[−2] | 3.9[−3]          | 1.1[−2]         | 1.7[−2]          |
| 20       | 8.8[−3] | 1.3[−2]         | 4.3[−2] | 8.2[−3]          | 2.6[−2]         | 4.0[−2]          |
| 40       | 1.7[−2] | 2.8[−2]         | 1.1[−1] | 1.7[−2]          | 6.1[−2]         | 1.1[−1]          |
|          | 1.7[−2] | 2.9[−2]         | 1.1[−1] | 1.8[−2]          | 6.2[−2]         | 1.2[−1]          |
| 60       | 2.4[−2] | 4.3[−2]         | 1.7[−1] | 2.4[−2]          | 1.0[−1]         | 1.7[−1]          |
| 80       | 3.1[−2] | 5.2[−2]         | 2.5[−1] | 3.2[−2]          | 1.4[−1]         | 2.6[−1]          |
| 100      | 3.8[−2] | 7.4[−2]         | 3.5[−1] | 4.0[−2]          | 1.9[−1]         | 3.7[−1]          |
|          | 3.9[−2] | 7.3[−2]         | 3.6[−1] | 4.0[−2]          | 2.0[−1]         | 3.5[−1]          |

time steps. Such trajectories proved sufficient to converge the self-diffusion coefficients and therefore the mutual diffusion within the Darken approximation [Eq. (25)], but not the mutual diffusion from the full MD simulation, especially the  $D_{\text{DLi}}$  component. For two representative temperatures with the 90-atom sample, we constructed a lengthy temporal trajectory by averaging eight independent simulation cases, each with approximately  $1.2 \times 10^5$  time steps with an effective total length of  $\approx 1 \times 10^6$  steps. The 40-eV temperature required a time step of 1.2 au (0.029 fs) and the 100 eV, of 0.7 au (0.0169 fs), yielding standard deviation in each of the RM Onsager coefficients ( $\Delta_{\text{DLi}}$ ,  $\Delta_{\text{DC}}$ ,  $\Delta_{\text{LiC}}$ ) of 6, 5, and 10%, respectively. However, the standard deviations of the mutual diffusion coefficients ( $D_{\text{DLi}}$ ,  $D_{\text{DC}}$ ) become almost a factor of four larger than those for the Onsager coefficients, namely 25% and 15%, respectively. On the other hand, the standard deviation in  $D_{\text{LiC}}$  remains at about 10%. The trends at 100 eV follow a similar pattern with the standard deviation error for the DLi, DC, and LiC RM Onsager coefficients yielding 6, 9, and 7%, respectively, while the errors in the mutual diffusion coefficients become 19, 19, and 8%. These findings seem to lend some credence to the adverse role played by Eqs. (13), (18), and (20) in amplifying the final error. Finally, the results, shown in the second row for these two temperatures in Table III, show excellent agreement with the Darken results.

Comparing Tables II and III for the Yukawa and OFMD, respectively, reveals that the mutual diffusion coefficients can disagree by as much as 90% at the lowest temperatures and by 20–30% by 100 eV. Given the agreement between the KS and OF at the lower temperatures, the difference in the Yukawa and OFMD establishes the merit of the former. This behavior could reflect the ability of the OF electronic density to respond over the whole system. Still, at this level, the Yukawa provides an effective guide to the general behavior of the mutual diffusion.

## 2. D-Li-Ag and H-C-Ag

We present calculations for a mixture of deuterium (D), lithium (Li), and silver (Ag) at a density of  $20 \text{ g/cm}^3$  for

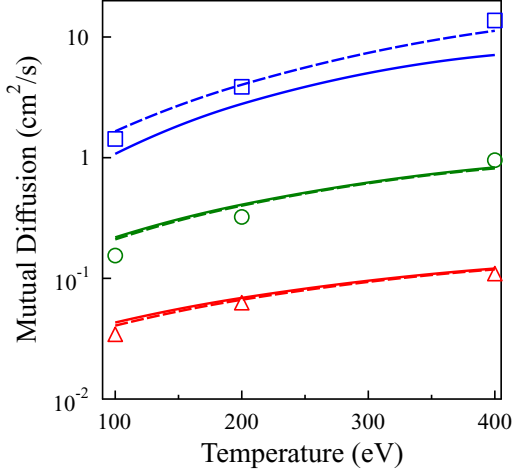


FIG. 5. Mutual diffusion coefficients as a function of temperature for D-Li-Ag for a 1:1:2 sample of 800 atoms at  $20 \text{ g/cm}^3$  result for coefficients DLi (blue upper group), DAg (green middle group), and LiAg (red lower group). Within each group: Yukawa model for full MD simulations (solid line) and Darken approximation (dash line); OFMD Darken results shown as symbols.

a range of temperatures at a 1:1:2 concentration using the Yukawa parameters in Table I. The simulation employed 800 atoms with time steps of between 0.07 and 0.2 au for total trajectories spanning lengths of  $3.60 \times 10^8$  to  $7.2 \times 10^8$  steps and times to 20 ns. The statistical error for the mutual diffusion coefficients remained less than 5%. In Fig. 5, we compare mutual diffusion coefficients for the full MD simulations (solid lines) and Darken model (dashed lines) for the Yukawa for DLi (blue), DAg (green), and LiAg (red). The DLi mutuals display differences of 50% while in the DAg and LiAg mutuals agree to better than 5%. We also make comparison in Fig. 5 with the OFMD Darken results (symbols). The agreement between the Yukawa and OFMD Darken results is rather interesting, being better for the DLi case than the full Yukawa with its own Darken. We should note that such a trend does not hold for the D-Li-C case at lower temperatures as witnessed by the results in Tables II and III. We also display a similar plot in Fig. 6 for the system of H-C-Ag. The trends follow those for the D-Li-Ag system. The slight crossing of the Yukawa full mutual and Darken case above 300 eV is within the error estimate at these temperatures.

Finally, we investigate in Fig. 7 the trend in the both the center-of-mass-frame Onsager  $\Lambda_{\text{DLi}}$  and mutual diffusion  $D_{\text{DLi}}$  coefficients between two light species (DLi) as a function of the mass of the heavy third component given by carbon ( $Z = 6$ ), aluminum (13), copper (29), and silver (47) at 100 eV for 1:1:2 concentration at a density of  $20 \text{ g/cm}^3$  for 800 atoms in the Yukawa formulation. For the Onsager coefficient, we note an interesting progression with heavier species. The coefficient for C as the heavy component has a distinctly monotonic increase with time. However, with Al, we begin to observe a slight change in sign, crossing zero at about 25 fs. For the heavier species (Cu and Ag), this transition occurs with ever decreasing time. Such changes can reflect caging effects or more complex diffusion behav-

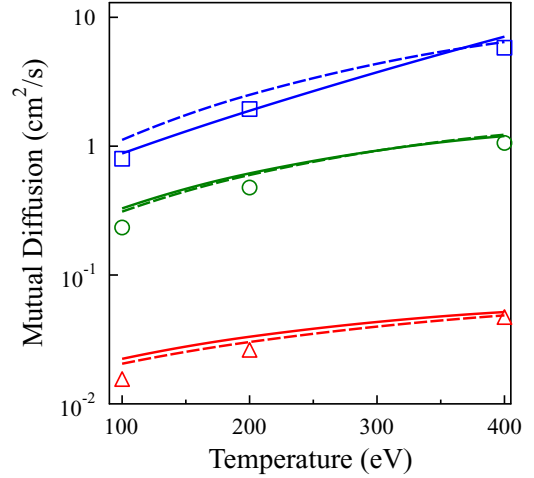


FIG. 6. Mutual diffusion coefficients as a function of temperature for H-C-Ag for 1:1:2 sample of 800 atoms at  $20 \text{ g/cm}^3$  result for coefficients HC (upper group, blue), HAg (middle group, green), and CAg (lower group, red); OFMD Darken results shown as symbols.

ior [64]. These small features also prove difficult to converge temporally and to fit. For the mutual diffusion coefficients (see the inset in Fig. 7), we note the steady rise of  $D_{\text{DLi}}$  with increasing mass of the heavy species as well as the increase in the width of the error bars (one standard deviation). For this exercise, we have fixed the mole concentrations, the mass density, and the temperature with the only variable the mass of the heavy species and concomitantly, the number density of the whole mixture. As the heavy species becomes more massive, the particle density declines. A lower density mixture usually facilitates greater diffusion so that we would generally expect  $D_{\text{LiD}}$  to increase. The behavior in the error bars further illustrates the convergence difficulty with increasing disparity in the system masses.

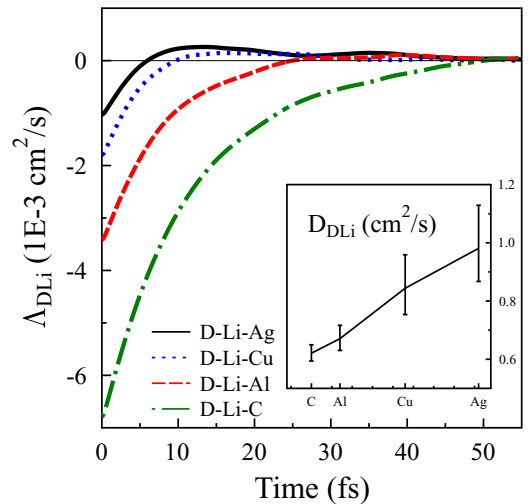


FIG. 7. Yukawa center-of-mass-frame Onsager  $\Lambda_{\text{DLi}}(t)$  [Eq. (9)] and mutual diffusion  $D_{\text{DLi}}$  (inset) coefficients for a DLiX mixture as a function of the heavier species  $X = \text{carbon } (Z = 6)$ , aluminum (13), copper (29), and silver (47) for  $20 \text{ g/cc}$  and a number concentration of 1:1:2 for 800 atoms at 100 eV. Error bars at 1 standard deviation.

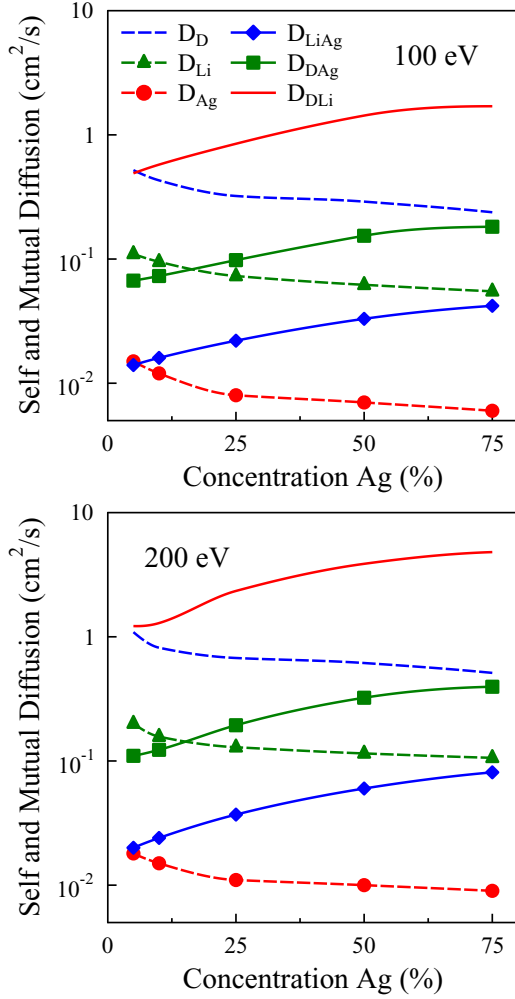


FIG. 8. OFMD self-diffusion and Darken mutual diffusion coefficients ( $\text{cm}^2/\text{s}$ ) for the ternary mixture D-Li-Ag at 100 eV (upper panel) and 200 eV (lower panel) for a fixed total pressure at each temperature as a function of concentration of the heavy species Ag. Labels:  $D_D$  (blue dashed line),  $D_{\text{Li}}$  (green dashed line and triangles),  $D_{\text{Ag}}$  (red dashed line and circles);  $D_{\text{DLi}}$  (red solid line),  $D_{\text{DAg}}$  (green solid line and squares), and  $D_{\text{LiAg}}$  (blue solid line and diamonds).

### B. Concentration dependence

We now change our emphasis and investigate the role played by concentrations of the various species. For this behavior, we found in the binary systems [22,23] that a different comparison scheme illuminated the effects more clearly, in particular that of isobaric equilibrium. We again consider ternary systems of two light species with a heavy companion, namely D-Li-Ag and H-C-Ag. In this case, we fix the temperature  $T$  and determine the total pressure  $P$  based on a  $20 \text{ g/cm}^3$  sample of D-Li-Ag (H-C-Ag) in a 1:1:2 number ratio. For the full sample, the relative concentrations of the light species remain fixed at equal amounts [ $x_D = x_{\text{Li}}$  and  $x_H = x_C$ ] and the concentration of the heavy species, in effect the mass density, varies under the constraint of constant  $T$  and  $P$  for a sample of 200 atoms.

For binary systems [22,23], the concentration of the heavy component had profound effects on the viscosity with small

increases causing a dramatic decrease. On the other hand, the mutual diffusion coefficients showed only a gradual rise with the heavy species concentration. The binary Darken relations [Eq. (23)] give a general characterization of this behavior. We consider a light (l) and heavy (h) species ( $m_l \ll m_h$ ) with  $x_h \rightarrow 1$ . In this case, the mutual diffusion coefficient depends almost entirely on the self-diffusion  $D_{lh} \rightarrow x_h D_l$ . In the opposite case, as  $x_h \rightarrow 0$ ,  $D_{lh} \rightarrow x_l D_h$ . Since usually  $D_l > D_h$ , the mutual diffusion coefficient will rise with an increase in  $x_h$ .

The ternary case presents more complicated relationships due to the interplay of the three different pairs of species. As with the binary case, we can gain some insight by employing the Darken forms, realizing that intra- and intercorrelation effects can alter the specifics. We consider the ternary Darken relations [Eq. (25)] for a system with two light species (1, 2) and one heavy (h) such that  $x_{11} = x_{12} \equiv x_l$  and  $D_{11} > D_{12} > D_h$ . As the heavy concentration increases ( $x_h \rightarrow 1$ ), the term  $D_m \rightarrow D_h/x_h$ , in which case the two coefficients connecting the light and heavy species behave much as in the binary case with  $D_{11h} \rightarrow x_h D_{11}$  and  $D_{12h} \rightarrow x_h D_{12}$ . On the other hand, the coefficient for the two light species has a different behavior  $D_{112} \rightarrow (x_h D_{11} D_{12})/D_h$ . For the reverse trend of  $x_h \rightarrow 0$ , we have  $D_{112} \rightarrow x_l D_{11}$ ;  $D_{11h} \rightarrow x_l \frac{(D_{11} D_h)}{D_{12}}$ , and  $D_{12h} \rightarrow x_l D_h$ .

Figure 8 examines these trends for the ternary systems by presenting the OFMD self ( $D_D$ ,  $D_{\text{Li}}$ ,  $D_{\text{Ag}}$ ) and the resulting Darken mutual ( $D_{\text{DLi}}$ ,  $D_{\text{DAg}}$ ,  $D_{\text{LiAg}}$ ) diffusion coefficients for the D-Li-Ag mixture as a function of the Ag concentration at two temperatures 100 eV (upper panel) and 200 eV (lower panel). As with the binary systems, the mutual diffusion coefficients monotonically rise as the heavy concentration and temperature increase. The increase with temperature follows directly from the enhanced collision frequency and mobility. We caution though that these trends derive from the Darken

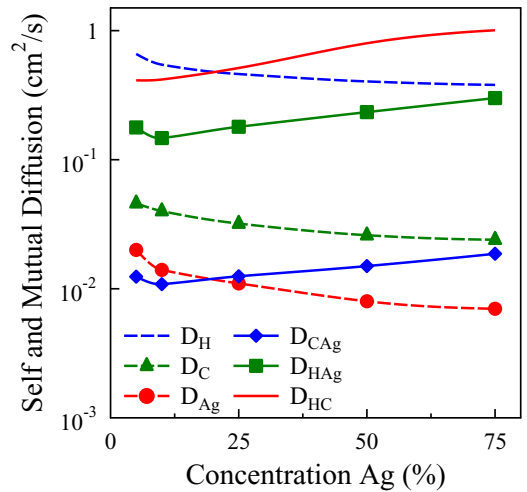


FIG. 9. OFMD self-diffusion and Darken mutual diffusion coefficients ( $\text{cm}^2/\text{s}$ ) for the ternary mixture H-C-Ag at 100 eV for a fixed total pressure at temperature of 100 eV as a function of concentration of the heavy species Ag. Labels:  $D_H$  (blue dashed line),  $D_C$  (green dashed line and triangles),  $D_{\text{Ag}}$  (red dashed line and circles);  $D_{\text{HC}}$  (red solid line),  $D_{\text{HAg}}$  (green solid line and squares), and  $D_{\text{CAg}}$  (blue solid line and diamonds).

relations, and since we employ the OFMD Darken coefficients, at least the behavior at the extremes ( $x_{\text{Ag}} = 0$  and 1) is innate to the formulation. The results generally follow the trends elucidated above. For example, assigning  $l_2$  to Li and  $h$  to Ag,  $D_{\text{LiAg}}$  approaches  $D_{\text{Li}}$  for  $x_{\text{Ag}} \rightarrow 1$  and  $D_{\text{Ag}}$  as  $x_{\text{Ag}}$  tends to zero. The mutual diffusion coefficient  $D_{\text{DAg}}$  with  $l_1(D)$  does approach  $D_D$  as the silver concentration rises. However, the behavior for small silver concentrations has a more complicated limit in terms of a fraction of the self-diffusion coefficients. Finally, Figure 9 displays the self and mutual diffusion coefficients for the H-C-Ag mixture as a function of the Ag concentration  $x_{\text{Ag}}$  at 100 eV. The results generally reinforce the findings for the Li-D-Ag system. We again observe that the mutual diffusion coefficient  $D_{\text{CAg}}$  between the intermediate light species (C) and the heavy species (Ag) tends to  $D_C$  at high silver concentrations and to  $D_{\text{Ag}}$  as  $x_{\text{Ag}} \rightarrow 1$ , but for the opposite limit, the behavior is more complicated. The self and mutual diffusion coefficients exhibit similar behavior as a function of  $x_{\text{Ag}}$  for 200 eV and 400 eV.

#### IV. CONCLUDING REMARKS

Our presentation included formulations, simulations, analysis, and results of calculations of mutual diffusion coefficients for mixtures in warm, dense matter regime. We focused on ternary systems and invoked the Born-Oppenheimer molecular dynamics scheme that evolved the ions classically and the electrons quantum mechanically through orbital-free density-functional theory as well as a classical MD approach with Yukawa pair-potentials, whose effective ionizations and electron screening length derive from quantal considerations. The trajectories, containing the positions and velocities of the ions as a function of time, determined various Onsager coefficients through autocorrelation functions, which in turn yielded the diffusion coefficients. Utilizing the RM formulation reduced the number of independent Onsager coefficients,

through its lack of dependence on a specific coordinate system. The full reference-frame-dependent Onsager terms arise from a similarity transformation. The RM formulation generally produced Onsager coefficients with less structure that more readily fit to simple analytical forms. We discovered that the diffusion coefficients required longer temporal trajectories ( $\approx 10^6 - 10^8$  time steps) to reach convergence than predicted from simple thermodynamical considerations. We examined as a function of temperature and mass density a representative sample of ternary mixtures from those with only light elements (D-Li-C) to those with highly asymmetric mass components (H-C-Ag) and also followed trends in the diffusion as a function of number concentration. We found that the Darken approximation, which neglects cross-correlations terms in the autocorrelation functions gives diffusion coefficients within 10–20% of the complete formulation for systems of light components and within a factor of two for highly asymmetric cases (e.g., H-C-Ag). The Maxwell-Stefan formulation provides a general prescription for determining diffusion coefficients in multispecies mixtures, applicable to classical and quantum mechanical molecular dynamics approaches. In this study, we have examined results for both a classical Yukawa potential and an orbital-free density functional approach. While in certain regimes, the classical approach may yield differences of a factor of two, the general trends in the diffusion coefficients are recovered.

#### ACKNOWLEDGMENTS

Work supported under the auspices of Science Campaigns 4 and 1 and the Advanced Technical Computing Campaign (ATCC) by the U.S. Department of Energy through the Los Alamos National Laboratory. Los Alamos National Laboratory is operated by Triad National Security, LLC, for the National Nuclear Security Administration of U.S. Department of Energy (Contract No. 89233218NCA000001).

- 
- [1] S. Hu, L. A. Collins, T. R. Boehly, Y. H. Ding, P. B. Radha, V. N. Concharov, V. V. Karasiev, G. W. Collins, S. P. Regan, and E. M. Campbell, *Phys. Plasmas* **25**, 056306 (2018), and reference therein.
  - [2] J. A. Gaffney, S. X. Hu, P. Arnault, A. Becker, L. X. Benedict *et al.*, *High Eng. Den. Phys.* **28**, 7 (2018).
  - [3] Y. H. Ding, A. J. White, S. X. Hu, O. Certik, and L. A. Collins, *Phys. Rev. Lett.* **121**, 145001 (2018).
  - [4] A. J. White, O. Certik, Y. H. Ding, S. X. Hu, and L. A. Collins, *Phys. Rev. B* **98**, 144302 (2018).
  - [5] T. Kluge, M. Rodel, J. Metzkes-Ng, A. Pelka, A. L. Garcia, I. Prencipe, M. Rehwald, M. Nakatsutsumi, E. E. McBride, T. Schonherr *et al.*, *Phys. Rev. X* **8**, 031068 (2018).
  - [6] V. Alopaeus and H. V. Norden, *Cmp. Chem. Eng.* **23**, 1177 (1999).
  - [7] M. Bethkenhagen, E. R. Meyer, S. Hamil, N. Nettleman, M. French, L. Scheibe, C. Ticknor, L. A. Collins, J. D. Kress, J. J. Fortney, and R. Redmer, *Astrophys. J.* **848**, 67 (2017).
  - [8] M. Millot, S. Hamel, R. Rygg, P. Celliers, G. Collins, F. Cooper, D. Fratanduomo, R. Jeanloz, D. Swift, and J. Eggert, *Nat. Phys.* **14**, 297 (2018).
  - [9] G. I. G. Griffiths, R. J. Needs, and C. J. Pickard, *Phys. Rev. B* **86**, 144102 (2012).
  - [10] M. Bethkenhagen, M. French, and R. Redmer, *J. Chem. Phys.* **138**, 234504 (2013).
  - [11] T. R. Mattsson and M. P. Desjarlais, *Phys. Rev. Lett.* **97**, 017801 (2006).
  - [12] B. Militzer and H. F. Wilson, *Phys. Rev. Lett.* **105**, 195701 (2010).
  - [13] M. Bethkenhagen, D. Cebulla, R. Redmer, and S. Hamel, *J. Phys. Chem. A* **119**, 10582 (2015).
  - [14] E. R. Meyer, C. Ticknor, M. Bethkenhagen, S. Hamel, R. Redmer, J. D. Kress, and L. A. Collins, *J. Chem. Phys.* **143**, 164513 (2015).
  - [15] *Exoplanet Science Strategy* (National Academy Press, Washington, DC, 2018).

- [16] D. A. Horner, J. D. Kress, and L. A. Collins, *Phys. Rev. B* **77**, 064102 (2008).
- [17] J. D. Kress, J. S. Cohen, D. A. Horner, F. Lambert, and L. A. Collins, *Phys. Rev. E* **82**, 036404 (2010).
- [18] L. Burakovsky, C. Ticknor, J. D. Kress, L. A. Collins, and F. Lambert, *Phys. Rev. E* **87**, 023104 (2013).
- [19] T. Haxhimali, R. E. Rudd, W. H. Cabot, and F. R. Graziani, *Phys. Rev. E* **90**, 023104 (2014).
- [20] L. G. Stanton and M. S. Murillo, *Phys. Rev. E* **91**, 033104 (2015).
- [21] J. D. Kress, C. Ticknor, and L. A. Collins, internal report, LAUR-15-27198 (2015).
- [22] C. Ticknor, J. D. Kress, L. A. Collins, J. Clerouin, P. Arnault, and A. Decoster, *Phys. Rev. E* **93**, 063208 (2016).
- [23] A. J. White, L. A. Collins, J. D. Kress, C. Ticknor, J. Clerouin, Ph. Arnault, and N. Desbiens, *Phys. Rev. E* **95**, 063202 (2017).
- [24] Z. G. Li, W. Zhang, Z.-J. Fu, J.-y. Dai, Q.-F. Chen, and X.-R. Chen, *Phys. Plasmas* **24**, 052903 (2017).
- [25] A. Becker, M. Bethkenhagen, C. Kellermann, J. Wicht, and R. Redmer, *Astronom. J.* **156**, 149 (2018).
- [26] C. Truesdell, *J. Chem. Phys.* **37**, 2336 (1962).
- [27] Y. Zhou and G. H. Miller, *J. Phys. Chem.* **100**, 5516 (1996).
- [28] D. R. Wheeler and J. Newman, *J. Phys. Chem. B* **108**, 18353 (2004).
- [29] X. Liu, T. J. H. Vlugt, and A. Bardow, *Fluid Phase Equilib.* **301**, 110 (2011).
- [30] J. W. Mutoru and A. Firoozabadi, *J. Chem. Thermo.* **43**, 1192 (2011).
- [31] X. Liu, S. K. Schnell, J.-M. Simon, P. Kruger, D. Bedeaux, S. Kjelstrup, A. Bardow, and T. J. H. Vlugt, *Int. J. Thermophys.* **34**, 1169 (2013).
- [32] M. Schoen and C. Hoheisel, *Mol. Phys.* **52**, 33 (1984).
- [33] R. Krishna and J. A. Wesselgh, *Chem. Eng. Sci.* **52**, 861 (1997).
- [34] C. F. Curtiss and R. B. Bird, *Ind. Eng. Chem. Res.* **38**, 2515 (1999).
- [35] D. Matuszak and M. D. Donohue, *Chem. Eng. Sci.* **60**, 4359 (2005).
- [36] R. Krishna and J. M. van Baten, *Ind. Eng. Chem. Res.* **44**, 6939 (2005).
- [37] X. Liu, T. J. H. Vlugt, and A. Bardow, *Ind. Eng. Chem. Res.* **50**, 10350 (2011).
- [38] X. Liu, S. K. Schell, J.-M. Simon, D. Bedeaux, S. Kjelstrup, A. Bardow, and T. J. H. Vlugt, *J. Phys. Chem. B* **115**, 12921 (2011).
- [39] X. Liu, A. Bardow, and T. H. J. Vlugt, *Ind. Eng. Chem. Res.* **50**, 4776 (2011).
- [40] X. Liu, A. Martin-Calvo, E. McGarrity, S. K. Schell, S. Calero, J.-M. Simon, D. Bedeaux, S. Kjelstrup, A. Bardow, and T. J. H. Vlugt, *Ind. Eng. Chem. Res.* **51**, 10247 (2012).
- [41] T. Janzen and J. Vrabec, *Ind. Eng. Chem. Res.* **57**, 16508 (2018).
- [42] R. Zwanzig and N. K. Ailawadi, *Phys. Rev.* **182**, 280 (1969).
- [43] P. Kruger, S. K. Schnell, D. Bedeaux, S. Kjelstrup, and T. J. H. Vlugt, *Phys. Chem. Lett.* **4**, 235 (2013).
- [44] N. Dawass, P. Kruger, S. K. Schnell, S. Kjelstrup, J. M. Simon, and T. J. H. Vlugt, *Mol. Sim.* **44**, 599 (2018).
- [45] J. C. Maxwell, *Phil. Trans. R. Soc.* **157**, 44 (1866); *The Scientific Papers of James Clerk Maxwell*, Vol. 2 (Dover, Dover, 1965), p. 26.
- [46] J. Stefan, *Sitz. ber., Akad. Wiss. Math.-Nat. wiss. Kl.*, **63** (1871); **65**, 323 (1872).
- [47] S. Bastea, *Phys. Rev. E* **71**, 056405 (2005).
- [48] J. Trullàs and J. A. Padró, *J. Chem. Phys.* **99**, 3983 (1993).
- [49] F. O. Raineri and H. L. Friedman, *J. Chem. Phys.* **91**, 5633 (1989).
- [50] M. P. Allen and D. J. Tildesley, *Computer Simulations of Liquids* (Oxford Science Publications, Oxford, 1987).
- [51] M. Pearson, E. Smargiassi, and P. A. Madden, *J. Phys.: Condens. Matter* **5**, 3221 (1993).
- [52] H. Ohta and S. Hamaguchi, *Phys. Plasmas* **7**, 4506 (2000).
- [53] F. Lambert, J. Clerouin, and G. Zerah, *Phys. Rev. E* **73**, 016403 (2006).
- [54] D. Giles, F. Lambert, J. Clerouin, and G. Salin, *High Energy Density Phys.* **3**, 95 (2007).
- [55] P. A. Bradley, E. N. Loomis, E. C. Merritt, J. A. Guzik, P. H. Denne, and T. T. Clark, *Phys. Plasmas* **25**, 012710 (2018).
- [56] S. Plimpton, *J. Comput. Phys.* **117**, 1 (1995).
- [57] F. Perrot, *Phys. Rev. A* **20**, 586 (1979).
- [58] J. P. Perdew and A. Zunger, *Phys. Rev. B* **23**, 5048 (1981).
- [59] J. D. Kress, J. S. Cohen, D. P. Kilcrease, D. A. Horner, and L. A. Collins, *Phys. Rev. E* **83**, 026404 (2011).
- [60] D. A. Horner, F. Lambert, J. D. Kress, and L. A. Collins, *Phys. Rev. B* **80**, 024305 (2009).
- [61] J. F. Daniel, L. Kazandjian, and G. Zerah, *Phys. Plasmas* **19**, 122712 (2012).
- [62] D. Sheppard, J. D. Kress, S. Crockett, L. A. Collins, and M. P. Desjarlais, *Phys. Rev. E* **90**, 063314 (2014).
- [63] S. X. Hu, B. Militzer, L. A. Collins, K. P. Driver, and J. D. Kress, *Phys. Rev. B* **94**, 094109 (2016).
- [64] E. R. Meyer, J. D. Kress, L. A. Collins, and C. Ticknor, *Phys. Rev. E* **90**, 043101 (2014).
- [65] F. Lambert and V. Recoules, *Phys. Rev. E* **86**, 026405 (2012).